Spatial and temporal variations in plant Water Use Efficiency inferred from tree-ring, eddy covariance and atmospheric observations

Stefan C. Dekker[1*], Margriet Groenendijk[2*], Ben B. B. Booth[3], Chris Huntingford[4] and Peter M. Cox[2]

* *These authors contributed equally to this work*

[1] *Copernicus Institute of Sustainable Development, Faculty of Geosciences, Utrecht University, Heidelberglaan 2, 3584 CS Utrecht, the Netherlands*

[2] *College of Engineering, Mathematics and Physical Sciences, University of Exeter, North Park Road, Exeter, EX4 4QF, UK*

[3] *Met Office Hadley Centre, FitzRoy Road, Exeter, EX1 3PB, UK*

[4] *Centre for Ecology and Hydrology, Benson Lane, Wallingford, OXON, OX10 8BB, UK*

Abstract

Plant Water Use Efficiency (*WUE*), which is the ratio of the uptake of carbon dioxide through photosynthesis to the loss of water through transpiration, is a very useful metric of the functioning of the land biosphere. *WUE* is expected to increase with atmospheric CO_2, but to decline with increasing atmospheric evaporative demand – which can arise from increases in near-surface temperature or decreases in relative humidity. We have used $\Delta^{13}C$ measurements from tree-rings, along with eddy-covariance measurements from Fluxnet sites, to estimate the sensitivities of WUE to changes in CO_2 and atmospheric humidity deficit. This enables us to reconstruct fractional changes in *WUE*, based on changes in atmospheric climate and CO_2, for the entire period of the instrumental global climate record. We estimate that overall *WUE* increased from 1900 to 2010 by 48±22%, which is more than double that simulated by the latest Earth System Models. This long-term trend is largely driven by increases in CO_2, but significant inter-annual variability and regional differences are evident due to variations in temperature and relative humidity. There are several highly populated regions, such as Western Europe and East Asia, where the rate of increase of *WUE* has declined sharply in the last two decades. Our data-based analysis indicates increases in *WUE* that typically exceed those simulated by Earth System Models – implying that these models are either underestimating increases in photosynthesis or underestimating reductions in transpiration.

1. Introduction

Plant Water Use Efficiency (*WUE*) is the ratio of the CO_2 assimilated through photosynthesis (Gross Primary Productivity, *GPP*), to the water used by plants as the flux of Transpiration (E_T):

$$WUE = \frac{GPP}{E_T} \quad (1)$$

Carbon dioxide may affect plants through increases in photosynthesis (Ainsworth and Rogers 2007; Franks et al. 2013) and possible reductions in transpiration associated with the partial closure of leaf stomatal pores under elevated CO_2 (Field et al. 1995; Gedney et al. 2006; Betts et al. 2007). Both of these effects are uncertain though. CO_2-fertilization of photosynthesis is often found to be limited by nutrient availability (Norby et al. 2010), and large-scale transpiration may not reduce even with CO_2-induced stomatal closure, if plant leaf area index increases enough to counteract reduced transpiration from each leaf (Piao et al. 2007). *WUE* does however appear to be increasing more robustly with CO_2, according to both tree-ring (Franks et al. 2013) and eddy-covariance flux measurements (Keenan et al. 2013).

Plant photosynthesis and transpiration are coupled through the behaviour of leaf stomatal pores, through which CO_2 must diffuse to be fixed during photosynthesis, and through which the transpiration flux escapes to the atmosphere. The combined behaviour of the leaf stomata leads to an environmentally dependent "canopy conductance" that controls both the water and carbon fluxes. As a consequence, both *GPP* and E_T can be written as the product of a canopy conductance and a

concentration gradient, which is sometimes described as an electrical analogue (Cowan 1972). For *GPP*, the concentration gradient is the difference between the atmospheric CO_2 concentration at the leaf surface (C_a) and the internal CO_2 concentration within plant leaves (C_i):

$$GPP = g_c(C_a - C_i) \quad (2)$$

where g_c is the canopy conductance for CO_2.

For E_T, the concentration gradient is the difference between the specific humidity of the atmosphere at the leaf surface (q_a) and the specific humidity inside the plant leaves, which is saturated at the leaf temperature (q_{sat}). The canopy conductances for *GPP* and E_T both arise from diffusion through leaf stomatal pores, and therefore only differ by a constant factor of 1.6 (the square root of the ratio of the molecular masses of CO_2 and H_2O).

$$E_T = 1.6 g_c(q_{sat} - q_a) \quad (3)$$

Changes in stomatal opening in response to changes in sunlight, atmospheric temperature and humidity, soil moisture, and CO_2, are complex and uncertain (Berry et al. 2010), as are the scaling of these leaf-level responses up to the canopy and beyond (Piao et al. 2007; Jarvis and McNaughton 1986; Jarvis 1995). However, since stomatal behaviour affects transpiration and photosynthesis similarly, *WUE* is relatively insensitive to these uncertainties:

$$WUE = \frac{(C_a - C_i)}{1.6(q_{sat} - q_a)} = \frac{(C_a - C_i)}{1.6D} = \frac{C_a(1-f)}{1.6D} \quad (4)$$

where D is the atmospheric humidity deficit (q_{sat}-q_a) and f is the ratio of the internal to the external CO_2 concentration (C_i/C_a). This equation therefore expresses WUE in terms of atmospheric variables, C_a and D (which itself depends on relative humidity and temperature), along with the factor f. The remaining uncertainty associated with plant physiology is therefore contained in f.

In the absence of water limitations, there is good evidence that f is approximately independent of C_a, so that C_i remains proportional to C_a, unless D changes (Jacobs 1994; Katul et al. 2010; Leuning 1995; Morison et al. 1983). Even during drought, f will vary with D, due in part to correlations between D and soil moisture (Brodribb 1996).

Stomatal optimisation theories, which assume that stomata act so as to maximise photosynthesis for a given amount of available water (Cowan and Farquhar 1977), also suggest that f should depend predominantly on C_a and D (Katul et al. 2010; Medlyn et al. 2011). Absolute values of WUE will depend on the nature of the vegetation and soil, such as the plant and soil hydraulics, but these optimisation theories imply that there will be a near universal sensitivity of fractional changes in WUE to fractional changes in C_a and D (see SI Appendix):

$$\frac{WUE}{WUE(0)} = \left(\frac{C_a}{C_a(0)}\right)^a \left(\frac{D}{D(0)}\right)^b \quad (5)$$

where the subscript (0) denotes the initial state of each variable, and a and b are dimensionless coefficients. For given a and b values this equation describes how the fractional change in WUE at each location varies with fractional changes in C_a and D. Although they differ in their underlying

assumptions and detailed conclusions, it is interesting to note that the latest stomatal optimization theories (Katul et al. 2010; Medlyn et al. 2011) both imply $a=1$ and $b=-0.5$ (see SI Appendix).

We focus in this study on fractional changes in *WUE*, which are more likely to be independent of these complex factors. Therefore, we use two very different datasets of *WUE*, derived from tree ring measurements and eddy-covariance fluxes and aim to model the fractional changes in plant *WUE* by using atmospheric data alone. The longer-term climate signals are derived from the tree rings, spanning at least the last 100 years. Monthly *WUE* values are derived from eddy-covariance observations between 1995-2006. We do not assume the applicability of stomatal optimization theories, but instead adopt equation 5 as a parsimonious empirical model for the fractional changes in *WUE* observed at each measurement site, given suitable fitting parameters a and b. Tests using more elaborate statistical models, with additional environmental variables or vegetation-specific parameters, were not found to produce significant improvements in the fit to the observed changes in *WUE* despite the introduction of extra fitting parameters. Finally, we have compared our reconstruction of the fractional change in plant *WUE* to Earth System Models (ESMs) simulations, focussing on regional variations in the *WUE* changes and how these compare to the long-term tree ring observations.

2. Materials and Methods

We estimate the sensitivity of *WUE* to C_a and *D* by fitting to *WUE* changes inferred from both eddy-covariance fluxes (relatively short records with high-temporal resolution) and carbon isotope records from tree-rings (longer-term records with annual resolution). We use observations from 28 eddy-covariance and 31 tree-ring sites (see Figure 1 and SI Appendix, Tables S1 and S2).

2.1 Eddy-covariance observations.

The carbon and water flux observations were taken from the *Free Fair-use* Fluxnet database (www.fluxdata.org) (Baldocchi 2008; Papale et al. 2006; Reichstein et al. 2005). We selected a total of 28 sites based on data availability (Table S1). Monthly *WUE* was estimated from Equation 1 with *GPP* used directly from the database (Reichstein et al. 2005). In general the total latent heat flux (*LE*) has contributions from interception loss, soil evaporation and transpiration. We follow previous studies (Dekker et al. 2001; Groenendijk et al. 2011; Keenan et al. 2013; Law et al. 2002) in assuming that the latent heat flux is dominated by transpiration during periods with no rain in the preceding two days, when the interception loss and soil evaporation are assumed small. Monthly average values of *GPP*, E_T, C_a, *D* and *T* were calculated from half-hourly observations (not gap-filled) during dry periods (*i.e.* no rain in the preceding two days) when *GPP* was larger than zero. To exclude periods with unrealistic *WUE* values due to the division by very small E_T values, we used only months during the growing season. Annual average growing season values were calculated from the months with an average temperature above 10^{o}C. Only sites with at least 6 annual values were used, resulting in a dataset of 222 annual growing season values of *WUE*, C_a and *D*. Data are used between 1995 and 2006. Fractional changes were calculated relative to the mean over the observational period for each of the sites, to enable comparison between sites.

145 **2.2. Tree-ring observations**.

146 To derive a longer-term relationship between the fractional change in *WUE* and variations in C_a and
147 D, we used $\Delta^{13}C$ tree-ring observations from 31 locations (Figure 1), ranging from 1900 to current,
148 as described in two previous studies (Franks et al. 2013, Hemming et al. 1998) (see SI Appendix,
149 Table S2). The discrimination of ^{12}C against ^{13}C ($\Delta^{13}C$) is estimated from the tree-ring samples
150 (Hemming et al. 1998; van der Sleen et al. 2015). The $\Delta^{13}C$ measurements can be used to estimate
151 the ratio of the internal to the external CO_2 concentration ($f=C_i/C_a$) using the relationship: $f = (\Delta^{13}C$
152 $-4.4)/ (27-4.4)$, where $\Delta^{13}C$ is in parts per thousand (‰), and C_a is taken from the Mauna Loa
153 atmospheric CO_2 record (Farquhar et al. 1989; Franks et al. 2013; Keeling et al. 1976). *WUE* is
154 estimated with Equation 4 using annual average growing season values of D from the CRU dataset,
155 taking the nearest pixel to each site (Harris et al. 2013). This large-scale dataset for D ensures
156 consistency among the sites, but may underestimate the finer spatial variation in D. As for the eddy-
157 covariance sites, we estimated the fractional changes relative to the mean over the observational
158 period at each of the sites. For this analysis we have 1007 observations of *WUE* derived from tree-
159 ring observations of $\Delta^{13}C$.

160

161 **2.3 Fractional WUE**

162 To estimate a and b with a linear regression model we rewrite Equation 5 in a logarithmic form:

163

164 $$\ln\left\{1+\frac{\Delta WUE}{WUE(0)}\right\} = a\ln\left\{1+\frac{\Delta C_a}{C_a(0)}\right\} + b\ln\left\{1+\frac{\Delta D}{D(0)}\right\} \quad (6)$$

165

166 Here the second-term in each bracket represents the fractional change in *WUE*, C_a and D, respectively.
167 These fractional change variables are used in all our subsequent statistical analyses and modelling.

168 We set out to fit the fractional change in *WUE* at each observation site (Figure 1) from the fractional
169 change in C_a and the fractional change in *D*. For comparison and fitting we therefore need to calculate
170 *WUE(0)*, $C_a(0)$ and *D(0)* for the observational data, which we take as the mean over the entire
171 observational record available at each site.
172
173 **2.4 Global fractional change of WUE**
174 The dependence of fractional changes in *WUE* on C_a and *D* allows us to use these relationships to
175 estimate changes in *WUE* at large scales using global climate data. The fractional change in *D* can be
176 further partitioned into a change in temperature (*T*) and relative humidity (*RH*), which makes it
177 possible to separate the effect of changes in these variables on *WUE* (see SI Appendix). To do this,
178 we used the CRU climate dataset (Harris et al. 2013) at a $0.5^o \times 0.5^o$ latitude/longitude grid and the
179 annual CO_2 concentration at Mauna-Loa (Keeling et al. 1976) to derive the global and local variation
180 in *WUE*. We only used months during the growing season when photosynthesis occurs, assumed to
181 be above a monthly average temperature threshold of 10^oC. For the period 1900-1930 the average
182 temperature was calculated for each month from which a spatial mask was generated (SI Appendix,
183 Fig. S4). This mask was then used to calculate annual time-evolving values of *WUE* from the growing
184 season values of temperature and humidity for each year between 1901 and 2010.
185
186 **2.5 Other independent data sources**
187 For three locations, Western North America, Western Europe and East Asia, we have compared our
188 simulated fractional change in plant WUE with remote sensing (RS) products of *GPP* and E_T (Jung
189 et al. 2011). This dataset covers the period 1982-2006; we use the period 1986-1990 as a reference
190 period for both our estimate and the fractional change in *WUE* from the RS product. As the RS data

191 does not cover a response to changes in C_a, we estimated the fractional change in *WUE* with and
192 without the C_a response.
193 At the global scale, we have compared our simulated fractional change in plant *WUE* with simulations
194 of Earth System Models (ESMs). Most of the latest ESMs calculate changes in both *GPP* and E_T.
195 This allows a comparable change in *WUE* to be calculated for 28 CMIP5 models (Taylor et al. 2012)
196 based-on their historical simulations. Finally, regional differences in responses are compared to the
197 31 tree ring observation sites.

198 **3 Results and Discussion**

199 Figure 2 summarises the derivation of the *a* and *b* parameters, which are the sensitivity of *WUE* to C_a
200 and *D*, for the tree-ring and eddy-covariance observations. In general, eddy-covariance data alone is
201 unable to fully constrain the CO_2 sensitivity of the *WUE* (Keenan et al. 2013), because the data records
202 are too short to sample significant changes in CO_2, resulting in a value of *a* of 0.79±0.79 for all eddy-
203 covariance site (SI Appendix, Fig. S1 and Table S3). However, the longer tree-ring records overall
204 yield a good constraint on *a* of 1.61±0.54. The annual data-points for the two datasets can be
205 combined into a single dataset. Fitting against this more complete dataset gives generic sensitivity
206 coefficients of *a*=1.51±0.57 and *b*=-0.72±0.16. These values are mainly constrained by the tree-ring
207 observations for which the fits to equation 6 are more tightly defined (Fig. 2a and SI Appendix, Fig
208 S1 top row).

209 A value of *a* larger then 1, suggests that *WUE* has been increasing even faster than the atmospheric
210 CO_2 concentration (Fig. 2c). This is qualitatively consistent with conclusions from a previous study,
211 which was based purely on eddy covariance data (Keenan et al. 2013), but is more robustly
212 demonstrated here due to the much longer tree-ring records.

213

214 It is interesting to note that our overall values of *a*=1.51±0.57 and *b*=-0.72±0.16 are larger by about
215 50% than the values derived from stomatal optimization theories: *a*=1.0, *b*=-0.5 (Cowan and Farquhar
216 1977; Katul et al. 2010; Palmroth et al. 2013), indicating a stronger response to changes in both CO_2
217 and climate. Such theoretical sensitivities are common to variants of stomatal optimization theory,
218 including those that assume either electron transport-limited or Rubisco-limited photosynthesis, and
219 even when additional nitrogen limitations are accounted for (Prentice et al. 2013). The differences
220 between the optimization theory and our empirically derived *WUE* sensitivities may arise from

differences between leaf-surface and atmospheric values of CO_2 and humidity, but they may also be indicative of missing constraints and feedbacks in the optimization theories (Lin et al. 2015; Prentice et al. 2014; de Boer et al. 2011, 2016).

Testing more elaborate statistical models.

Equation 6 is motivated by empirical evidence and theory suggesting that *WUE* should vary predominantly with C_a and D. However, it is conceivable that the fractional change in *WUE* could also depend on other environmental conditions or the detailed vegetation type. In order to test for this, we carried out two additional sets of fits against the observational data. In the first test we extended our statistical model (equation 6) to include other environmental variables that had been measured at the *Fluxnet* sites, most notably solar radiation, air temperature, and soil water content. Including these additional predictor variables does not significantly improve the fit to the observed changes in *WUE* (as measured by r^2), and typically results in less robust predictions (as measured by the adjusted r^2), because of the introduction of extra fitting parameters (SI Appendix, Table S4). In the second test, we carried out separate statistical fits for each of the sites listed in the *Fluxnet* dataset. Clustering of these values by vegetation type would indicate that a and b parameters are dependent on vegetation type, but we find no evidence of such clustering (Figure 3).

Comparison to independent *WUE* estimates.

Our best-fit generic a and b parameters are able to reasonably reproduce the fractional changes in *WUE* due to fractional changes in both C_a and D across the 59 tree-ring and eddy-covariance sites (SI Appendix, Fig. S2). However, it is important to evaluate the estimated response of *WUE* to C_a and D against independent data. We compared the change in *WUE* estimated with the best-fit parameters to

observations at three tropical tree-ring sites from a recent study (van der Sleen et al. 2015). At these sites a range of species of both trees and under-storey were sampled. Our estimate for these three locations passes close to the mean of the observed *WUE* fractional changes (Fig. 4a-c). Because the RS data does not include a response to changes in C_a, we estimated a fractional change in *WUE* with and without this response (Fig. 4d-f) for three regions, which show distinct changes in *WUE*: Western North America, Western Europe and East Asia. The RS fluxes show little inter-annual variability, and much less variability than we estimate. For the three regions in Fig. 4d-f our estimates with and without CO_2 effects sit on either side of the RS estimates. In the Amazon, South Africa and South East Asia (see SI Appendix, Fig. S3) our estimates excluding CO_2 effects are similar to the RS estimates, whilst the inclusion of CO_2 effects leads to significant increases in WUE (SI Appendix, Fig. S3) that appear to be inconsistent with the RS estimates (which do not account for CO_2 changes), but are more consistent with the tree-ring (Franks et al. 2013) and eddy-covariance data (Keenan et al. 2013).

Global fractional change of *WUE*.

Globally, we estimate that *WUE* has increased by 48±22% since 1900 (Fig. 5a), with the CO_2 increase contributing +47±21% and relative humidity contributing +3.6±1.3%, counteracted by a much smaller reduction in *WUE* due to warming of -2.3±0.8%. Estimated fractional changes in *WUE* between 1901-1930 and 2001-2010 differ regionally between 0.1 and 0.6 (Fig. 5b). Uncertainties in global *WUE* changes were derived from the range of the parameters *a* and *b* within 5% of the RMSE of our best fit (Fig. 2c).

Comparison to simulations with complex Earth System Models (ESMs).

The CMIP5 models simulate an increase in *WUE* of between 2% and 28% to 2005, with an ensemble mean of 14% (SI Appendix, Table S5). For comparison, our overall fit against the tree-ring and eddy-covariance data indicates an approximately 40% increase in *WUE* over the same period. Figure 6 compares the annual time-series of the fractional changes in *WUE* from the CMIP5 models (black line and green uncertainty plumes), our statistical fit (orange lines), and the mean changes observed for the tree-ring (black marks and grey uncertainty bars) and eddy-covariance sites (dark blue marks and light blue uncertainty bars). This comparison suggests that the latest ESMs significantly underestimate the historical increase in *WUE*.

Regional changes in *WUE*.

Our global average change in *WUE* hides substantial regional differences (Fig. 5b). This is a result of the spatially and temporally varying impact of climate change on *WUE* (Fig. 7a and animation in the Supporting Information), driven by the heterogeneity of the warming (Fig. 7b) and the large variation in changes in near-surface *RH* (Fig. 7c). In many regions the overall impact is a significant increase in *WUE*, such as Western North America (Fig. 7d). However, the recent rate of increase has declined substantially in several heavily populated regions. For example, *WUE* shows a slower increase in Western Europe since the 1980s, as a result of increases in *T*, which has counteracted the *WUE* increase due to increasing CO_2 (Fig. 7e). This is also observed in *WUE* trends derived from isotopic tree-ring observations in Spain (Linares et al. 2012). Our analysis indicates that East Asia has suffered an even more significant suppressions of *WUE* since about 1990, due predominantly to reductions in *RH* (Wang et al. 2012) (Fig. 7f). This pattern of changing *RH* is comparable with the trends in precipitation and drought since 1950 (Dai 2011).

289 For the 31 tree ring observation sites, we have plotted the ensemble mean regional ESM model results
290 against the individual observed tree ring data (Fig. S5). For 10 out of 31 observation sites, the
291 simulated fractional *WUE* increases between 5-10%. For 3 out of the 31 sites, the fractional *WUE*
292 increases by more than 50%, and for 14 out of the 31 observation sites the *WUE* change inferred from
293 the tree ring data is significantly higher than that simulated by the ESMs.
294

4. Conclusions

This study shows that fractional changes in plant *WUE*, at large-scales and over the period of the climatological record, can be inferred from atmospheric data alone. By combining two very different datasets of *WUE* derived from tree-ring $\Delta^{13}C$ measurements and eddy-covariance fluxes we have derived a consistent response of the fractional change in *WUE* to the fractional changes in C_a and D. This generic response can be used to estimate *WUE* changes over the entire period of the atmospheric record. Our analysis shows that global *WUE* increased by approximately a half over the 20th century predominantly due to rising CO_2, which is significantly more than is simulated by the latest Earth System Models. However, this increase in *WUE* has been modulated downwards in recent decades by the impact of climate change. This is especially true for the highly populated regions of Western Europe and East Asia, where reductions in atmospheric relative humidity and increases in temperature have acted to offset increases in *WUE* due to increasing CO_2. We conclude that the effects of increasing CO_2 on plant *WUE* are significantly underestimated in the latest climate projections.

ACKNOWLEDGEMENTS

The contributions of M.G.,C.H and P.C. were funded by the UK Natural Environment Research Council (NERC) HYDRA project. We thank Margaret Barbour for providing us tree-ring data compiled from many different sources. This work used eddy-covariance data acquired by the FLUXNET community and in particular by the following networks: AmeriFlux (U.S. Department of Energy, Biological and Environmental Research, Terrestrial Carbon Program (DE-FG02-04ER63917 and DE-FG02-04ER63911)), AfriFlux, AsiaFlux, CarboAfrica, CarboEuropeIP, CarboItaly,

CarboMont, ChinaFlux, Fluxnet-Canada (supported by CFCAS, NSERC, BIOCAP, Environment Canada, and NRCan), GreenGrass, KoFlux, LBA, NECC, OzFlux, TCOS-Siberia, USCCC. We acknowledge the financial support to the eddy covariance data harmonization provided by CarboEuropeIP, FAO-GTOS-TCO, iLEAPS, Max Planck Institute for Biogeochemistry, National Science Foundation, University of Tuscia, Université Laval and Environment Canada and US Department of Energy and the database development and technical support from Berkeley Water Center, Lawrence Berkeley National Laboratory, Microsoft Research eScience, Oak Ridge National Laboratory, University of California - Berkeley, University of Virginia.

328

329 **References**

330

331

332 Ainsworth EA, Rogers A (2007) The response of photosynthesis and stomatal conductance to rising
333 [CO2]: mechanisms and environmental interactions. Plant Cell Environ 30:258–270.

334 Baldocchi DD (2008) Breathing of the terrestrial biosphere: lessons learned from a global network of
335 carbon dioxide flux measurement systems. Aust J Bot 56:1–26.

336 Berry J, Beerling DJ, Franks PJ (2010) Stomata: key players in the earth system, past and present.
337 Curr Opin Plant Biol 13:233–240.

338 Betts RA Boucher O, CollinsM, Cox PM, Falloon PD, Gedney N, Hemming DL, Huntingford C,
339 Jones CD, Sexton DMH et al. (2007) Projected increase in continental runoff due to plant
340 responses to increasing carbon dioxide. Nature 448:1037–U5.

341 de Boer HJ, Lammertsma EI, Wagner-Cremer F, Dilcher DL, Wassen MJ and Dekker SC. 2011.
342 Climate forcing due to optimization of maximal leaf conductance in subtropical vegetation under
343 rising CO2. PNAS, Proc Natl Acad Sci USA 108:4041–4046.

344 de Boer HJ, Price CA, Wagner-Cremer F, Dekker, SC, Franks, PJ, Veneklaas EJ, 2016. Optimal
345 allocation of leaf epidermal area for gas exchange. New Phytol. 1219–1228.
346 doi:10.1111/nph.13929

347 Brodribb T (1996) Dynamics of changing intercellular CO2 concentration (ci) during drought and
348 determination of minimum functional ci. Plant Physiol 111:179–185.

349 Cowan I, Farquhar G (1977) Stomatal function in relation to leaf metabolism and environment. Soc
350 Exp Biol Symp 31:471–505.

Cowan IR (1972) An electrical analogue of evaporation from, and flow of water in plants. Planta 106:221–226.

Dai A (2011) Drought under global warming: a review. Wires Clim Change 2:45–65.

Dekker SC, Bouten W, Schaap MG (2001). Analysing forest transpiration model errors with artificial neural networks. Journal of Hydrology 246: 197-208.

Farquhar G, Ehleringer JR, Hubick KT (1989) Carbon isotope discrimination and photosynthesis. Annu Rev Plant Physiol Plant Mol Biol 40:503–537.

Field CB, Jackson RB, Mooney H (1995) Stomatal responses to increased CO_2: implications from the plant to the global-scale. Plant Cell Environ 18:1214–1225.

Franks PJ, Adams MA, Amthor JS, Barbour MM, Berry JA, Ellsworth DS, Farquhar GD, Ghannoum O, Lloyd J, McDowell N, et al. (2013) Sensitivity of plants to changing atmospheric CO_2 concentration: from the geological past to the next century. New Phytol 197:1077–1094.

Gedney N, Cox, PM, Betts, RA, Boucher, O, Huntingford, C, Stott, PA. (2006) Detection of a direct carbon dioxide effect in continental river runoff records. Nature 439:835–838.

Groenendijk M Dolman, A.J., Ammann, C., Arneth, A., Cescatti, A., Dragoni, D., Gash, J.H.C., Gianelle, D., Gioli, B., Kiely, G., Knohl, A., Law, B.E., Lund, M., Marcolla, B., Van Der Molen, M.K., Montagnani, L., Moors, E., Richardson, A.D., Roupsard, O., Verbeeck, H., Wohlfahrt, G., (2011) Seasonal variation of photosynthetic model parameters and leaf area index from global Fluxnet eddy covariance data. J Geophys Res 116.

Harris I, Jones PD, Osborn TJ, Lister DH (2013) Updated high-resolution grids of monthly climatic observations-the CRU TS3.10 Dataset. Int J Climatol.

372 Hemming DI, Switsur VR, Waterhouse JS, Heaton THE, Carter AHC (1998) Climate variation and
373 the stable carbon isotope composition of tree ring cellulose: an intercomparison of Quercus robur
374 , Fagus sylvatica and Pinus silvestris. Tellus B 50.
375 Jacobs CMJ (1994) Direct impact of atmospheric CO2 enrichment on regional transpiration.
376 Dissertation (Wageningen).
377 Jarvis PG (1995) Scaling processes and problems. Plant Cell Environ 18:1079–1089.
378 Jarvis PG, McNaughton KG (1986) Stomatal control of transpiration - Scaling up from leaf to region.
379 Adv Ecol Res 15:1–49.
380 Jung M, Reichstein, M., Margolis, H.A., Cescatti, A., Richardson, A.D., Arain, M.A., Arneth, A.,
381 Bernhofer, C., Bonal, D., Chen, J., Gianelle, D., Gobron, N., Kiely, G., Kutsch, W., Lasslop, G.,
382 Law, B.E., Lindroth, A., Merbold, L., Montagnani, L., Moors, E.J., Papale, D., Sottocornola, M.,
383 Vaccari, F., Williams, C., (2011) Global patterns of land-atmosphere fluxes of carbon dioxide,
384 latent heat, and sensible heat derived from eddy covariance, satellite, and meteorological
385 observations. J Geophys Res 116.
386 Katul G, Manzoni S, Palmroth S, Oren R (2010) A stomatal optimization theory to describe the effects
387 of atmospheric CO2 on leaf photosynthesis and transpiration. Annals of Botany 105:431–442.
388 Keeling CD, Bacastow, R.B., Bainbridge, A.E., Ekdahl Jr., C.. A., Guenther, P.R., Waterman, L.S.,
389 Chin, J.F.S., (1976) Atmospheric carbon dioxide variations at Mauna Loa Observatory, Hawaii.
390 Tellus 28:538–551.
391 Keenan TF Hollinger, D.Y., Bohrer, G., Dragoni, D., Munger, J.W., Schmid, H.P., Richardson, A.D.,
392 Keeling, B.C.D., Bacastow, R.B., Bainbridge, A.E., Ekdahl, C.A., Guenther, P.R., Waterman,
393 L.E.E.S. (2013) Increase in forest water-use efficiency as atmospheric carbon dioxide
394 concentrations rise. Nature 499:324–327.

395 Law, B.E., Falge, E., Gu, L., Baldocchi, D.D., Bakwin, P., Berbigier, P., Davis, K., Dolman, A.J.,
396 Falk, M., Fuentes, J.D., Goldstein, A., Granier, A., Grelle, A., Hollinger, D., Janssens, I.A., Jarvis,
397 P., Jensen, N.O., Katul, G., Mahli, Y., Matteucci, G., Meyers, T., Monson, R., Munger, W.,
398 Oechel, W., (2002) Environmental controls over carbon dioxide and water vapor exchange of
399 terrestrial vegetation. Agric For Meteorol 113:97–120.
400 Leuning R (1995) A critical appraisal of a combined stomatal-photosynthesis model for C3 plants.
401 Plant Cell Environ 18:339–355.
402 Lin, Y.-S., Medlyn, B.E., Duursma, R.A., Prentice, I.C., Wang, H., Baig, S., Eamus, D., de Dios,
403 V.R., Mitchell, P., Ellsworth, D.S., de Beeck, M.O., Wallin, G., Uddling, J., Tarvainen, L.,
404 Linderson, M.-L., Cernusak, L.A., Nippert, J.B., Ocheltree, T.W., Tissue, D.T., Martin-StPaul,
405 N.K., Rogers, A., Warren, J.M., De Angelis, P., Hikosaka, K., Han, Q., Onoda, Y., Gimeno, T.E.,
406 Barton, C.V.M., Bennie, J., Bonal, D., Bosc, A., Löw, M., Macinins-Ng, C., Rey, A., Rowland,
407 L., Setterfield, S.A., Tausz-Posch, S., Zaragoza-Castells, J., Broadmeadow, M.S.J., Drake, J.E.,
408 Freeman, M., Ghannoum, O., Hutley, L.B., Kelly, J.W., Kikuzawa, K., Kolari, P., Koyama, K.,
409 Limousin, J.-M., Meir, P., Lola da Costa, A.C., Mikkelsen, T.N., Salinas, N., Sun, W., Wingate,
410 L., 2015. Optimal stomatal behaviour around the world. Nat. Clim. Chang. 5, 459–464.
411 doi:10.1038/nclimate2550
412 Linares JC, Camarero JJ (2012) From pattern to process: linking intrinsic water-use efficiency to
413 drought-induced forest decline. Global Change Biology 18:1000–1015.
414 Medlyn BE Duursma, R.A., Eamus, D., Ellsworth, D.S., Prentice, I.C., Barton, C.V.M., Crous, K.Y.,
415 De Angelis, P., Freeman, M., Wingate, L., 2011. Reconciling the optimal and empirical
416 approaches to modelling stomatal conductance. Glob. Chang. Biol. 17, 2134–2144.
417 doi:10.1111/j.1365-2486.2010.02375.x

418 Morison JIL, Gifford RM (1983) Stomatal sensitivity to carbon dioxide and humidity. Plant Physiol
419 71:789–796.
420 Norby RJ, Warren JM, Iversen CM, Medlyn BE, McMurtrie RE (2010) CO_2 enhancement of forest
421 productivity constrained by limited nitrogen availability. P Natl Acad Sci Usa 107:19368–19373.
422 Palmroth S, Katul, G.G., Maier, C.A., Ward, E., Manzoni, S., Vico, G (2013) On the complementary
423 relationship between marginal nitrogen and water-use efficiencies among Pinus taeda leaves
424 grown under ambient and CO2-enriched environments. Annals of Botany 111:467–477.
425 Papale, D., Reichstein, M., Aubinet, M., Canfora, E., Bernhofer, C., Kutsch, W., Longdoz, B.,
426 Rambal, S. (2006) Towards a standardized processing of Net Ecosystem Exchange measured with
427 eddy covariance technique: algorithms and uncertainty estimation. Biogeosciences 3:571–583.
428 Piao, S., Friedlingstein, P., Ciais, P., de Noblet-Ducoudre, N., Labat, D. and Zaehle, S. (2007)
429 Changes in climate and land use have a larger direct impact than rising CO2 on global river runoff
430 trends. P Natl Acad Sci Usa 104:15242–15247.
431 Prentice IC, Dong N, Gleason SM, Maire V, Wright IJ (2014) Balancing the costs of carbon gain and
432 water transport: testing a new theoretical framework for plant functional ecology. Ecol Letters
433 17:82–91.
434 Reichstein M et al. (2005) On the separation of net ecosystem exchange into assimilation and
435 ecosystem respiration: review and improved algorithm. Global Change Biol 11:1424–1439.
436 Taylor KE, Stouffer RJ, Meehl G (2012) An Overview of CMIP5 and the Experiment Design, Bull.
437 Am. Meteorol. Soc., 93, 485–498, doi:10.1175/BAMS-D-11-00094.1.
438 van der Sleen P et al. (2015) No growth stimulation of tropical trees by 150 years of CO2 fertilization
439 but water-use efficiency increased. Nature Geoscience 8:24–28.

Wang K, Dickinson RE, Liang S (2012) Global atmospheric evaporative demand over land from 1973 to 2008. J Climate 25:8353–8361.

Figure Legends:

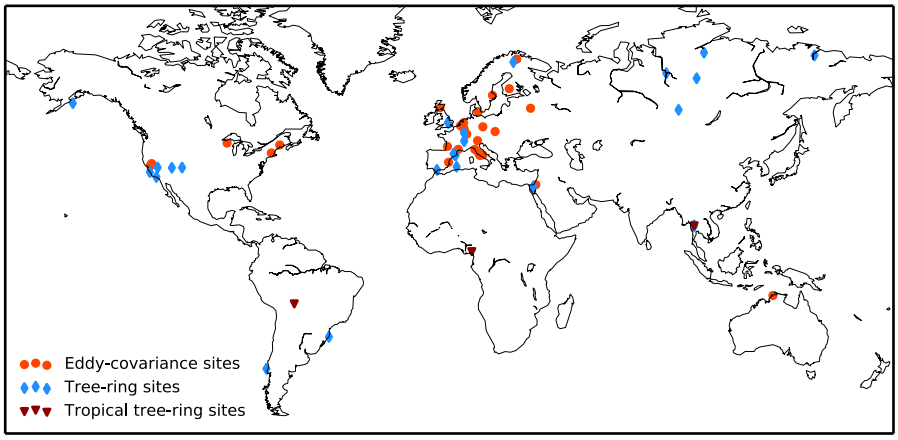

Figure 1. Locations of the eddy-covariance flux sites and tree-ring sites used (see Table S2 and S3 for a list of the sites). Tropical tree-ring sites are used as independent data sources for comparison.

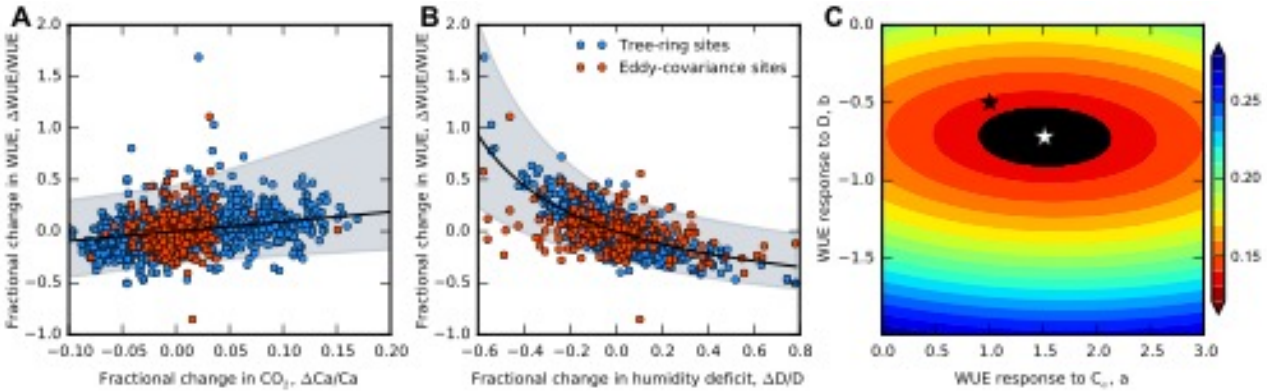

Figure 2. Water Use Efficiency (*WUE*) from tree-ring and eddy-covariance observations. The relationship between the observed fractional change in *WUE* and the fractional change in (A) CO_2 concentration and (B) humidity deficit of both datasets is fitted to Equation 3,with best-fit values for *a* (1.51±0.57) and *b* (-0.72±0.16). (C) The colors show the root mean square error (RMSE) of the simulated vs. observed fractional change in WUE as a function of *a* and *b*, with the black area representing the best parameters within 5% of the RMSE of the best fit (white star). The black star represents the values according to the optimality hypothesis.

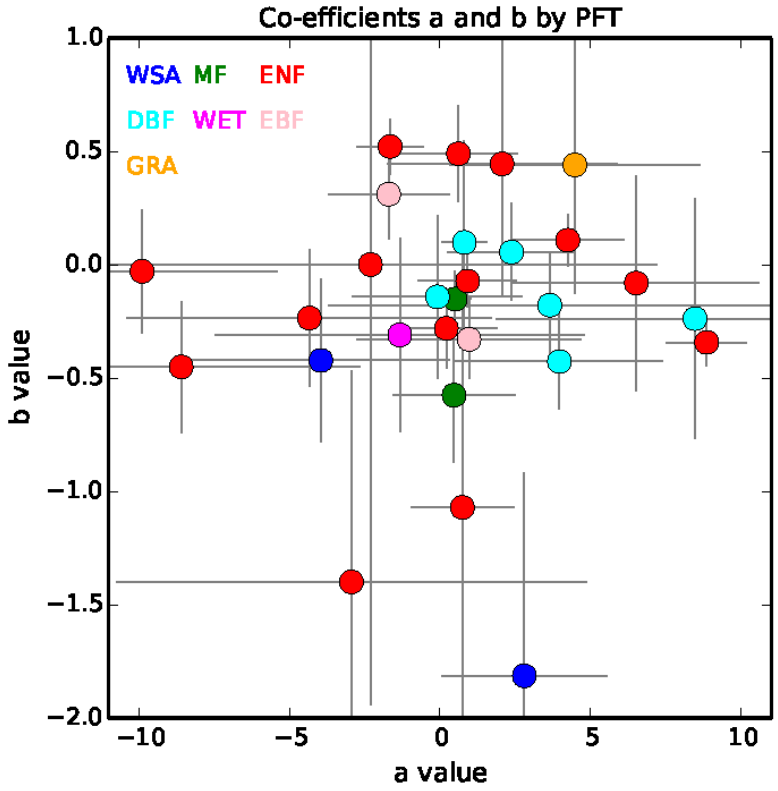

455

456 **Figure 3.** Comparison of best-fit a and b parameters (see equation 5) by plant functional type (PFT).
457 Here the sites are organized by dominant PFT, using classifications used for the FluxNet sites:
458 evergreen broadleaf forest (EBF), evergreen needleleaf forest (ENF), grassland (GRA), mixed forest
459 (MF), wetland (WET) and woody savannah (WSA).

460

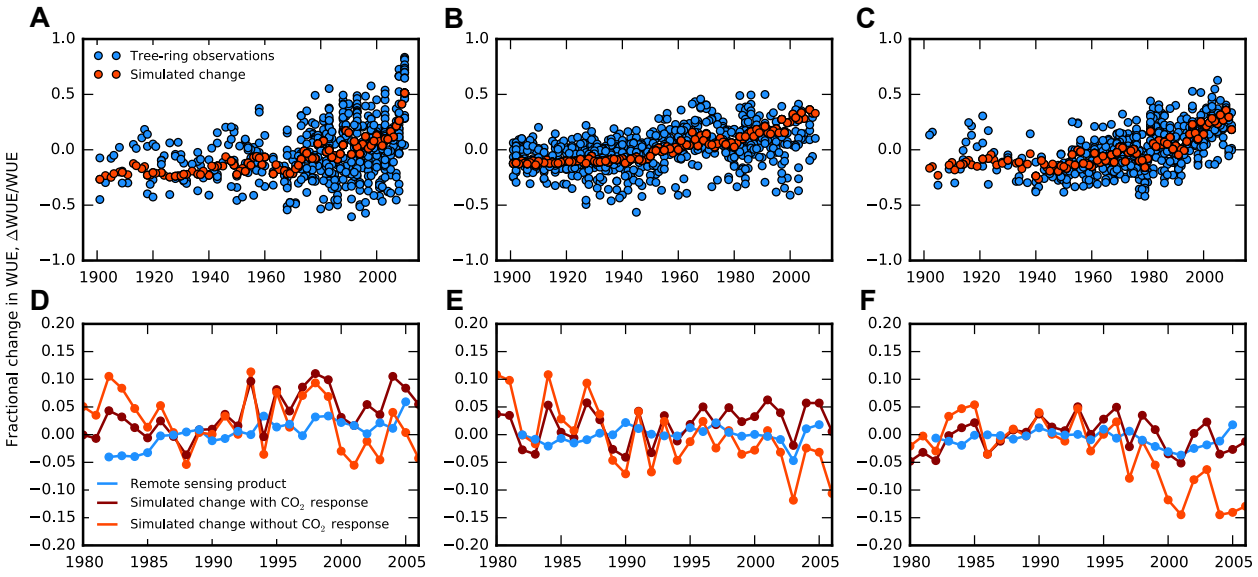

Figure 4. Comparison of estimated Water Use Efficiency trends to independent observations. Simulated fractional change in *WUE* (orange) compared to observations for three tropical tree-ring sites in Bolivia (A), Cameroon (B) and Thailand (C) (blue, van der Sleen 2015). Simulated fractional change in *WUE* for (D) Western North America, (E) Western Europe and (F) East Asia, with (dark red) and without (orange) CO_2 effect, compared to the *WUE* trend derived from a remote sensing product of carbon uptake and water loss (Jung et al. 2011). The location of the tree-ring sites is presented in Fig. S1 and the regions D-F are as in Fig. 5.

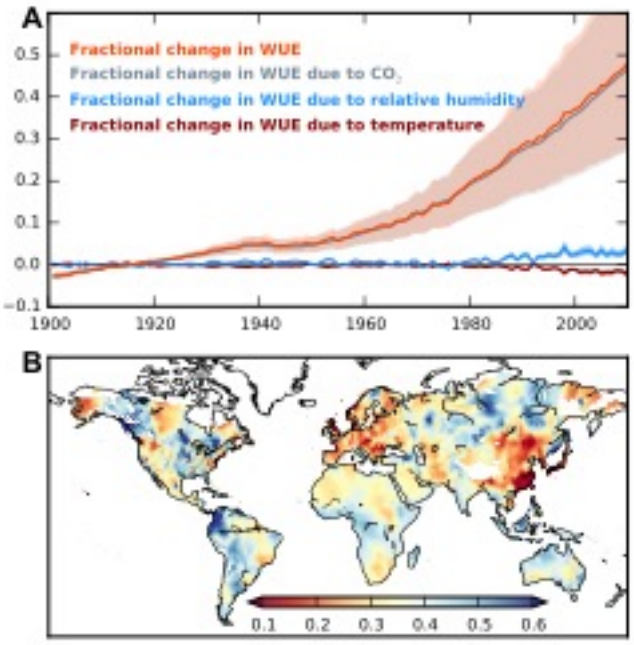

Figure 5. 20th century fractional change of Water Use Efficiency (*WUE*). (A) Time series of the estimated global fractional change in *WUE* (orange, relative to the average over 1901-1930) partitioned into the effects of changes in CO_2, relative humidity and temperature. (B) Spatial pattern of the estimated fractional change in *WUE* between 1901-1930 and 2001-2010. These calculations use observed monthly surface air temperature and vapour pressure (Harris et al. 2013) during the growing season, and annual atmospheric CO_2 concentrations at Mauna Loa (Keeling et al. 1976).

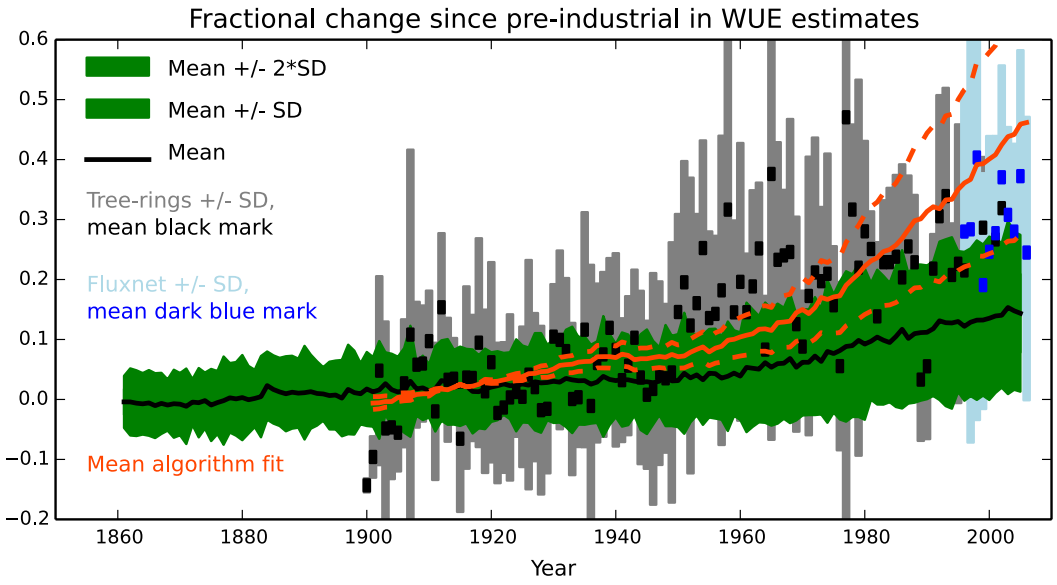

Figure 6. Comparison of measured and modeled fractional changes in *WUE* from 1860 to 2010. Estimates from tree-rings and eddy-covariance data are shown by the black and blue points respectively, with the bars in each case showing +/-1 standard deviation about the mean response. The results from complex coupled Earth System Models are shown by the black continuous line and the green plume (with dark green showing one standard deviation and light green showing two standard deviations). The algorithm presented in this paper, which estimates fractional *WUE* changes from changes in CO_2 concentration and humidity deficit alone (equation 6), is shown by the orange lines. To enable the comparison between these different estimates, we normalized over common overlapping periods (for the tree-ring data and model simulations – 1900-1930; for the tree-ring and eddy-covariance data – the period of overlap when at least 3 eddy-covariance sites are available).

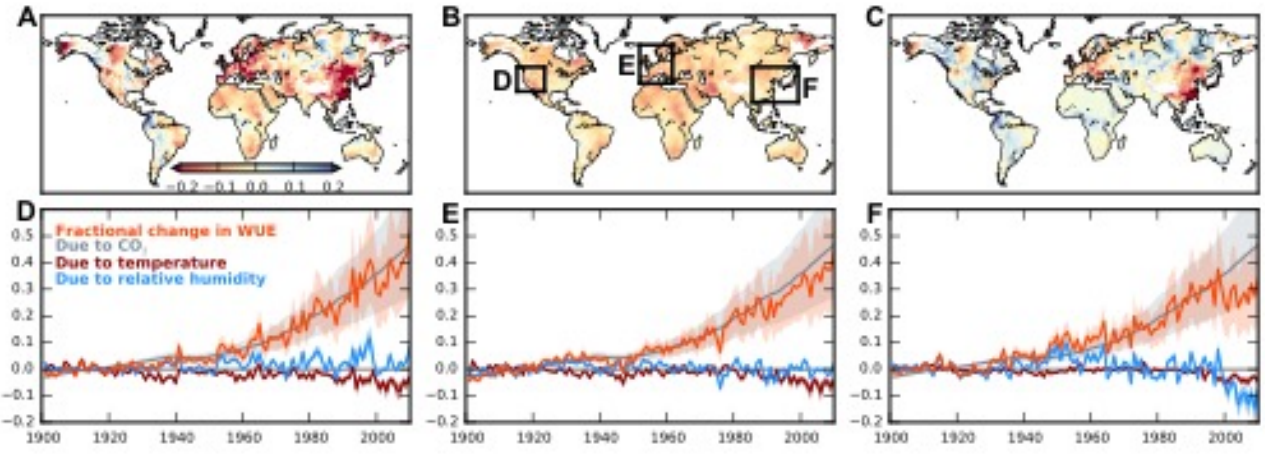

492

493 **Figure 7.** Changes in *WUE* arising from climate variables. Spatial patterns of the fractional changes
494 in WUE arising from changes in (A) climate, i.e. both temperature and relative humidity (*RH*)
495 together, (B) temperature alone, and (C) *RH* alone, between 1901-1930 and 2001-2010. Time-series
496 are as in Fig. 5 for (D) Western North America, (E) Western Europe and (F) East Asia, which show
497 the large regional and temporal variations in these climate-driven changes in *WUE*.